ORIGINAL ARTICLE

Additively manufactured cure tools for composites manufacture

Max D. A. Valentine[1] · Arjun Radhakrishnan[2] · Vincent K. Maes[2] · Elise C. Pegg[1] · Maria D. R. Valero[3] · James Kratz[2] · Vimal Dhokia[1]

Abstract

This research presents a novel framework for the design of additively manufactured (AM) composite tooling for the manufacture of carbon fibre-reinforced plastic composites. Through the rigorous design and manufacture of 30 unique AM tools, the viability of a design for AM framework was evaluated through measuring the performance with respect to geometrical accuracy and thermal responsiveness, and simulating the tool specific stiffness. The AM components consisted of a thin layup facesheet, stiffened by a low density lattice geometry. These tools were successfully used to layup and cure small composite components. The tooling was highly thermally responsive, reaching above 93% of the applied oven heating rate and up to 17% faster heating rates compared to similar mass monolithic tools. The results indicate that thermal overshoot has a greater dependence on the lattice density while the heating rate was more sensitive to the facesheet thickness. Lattice densities of as little as 5% were manufactured and the best overall geometry was a graded gyroid lattice with thicker walls near the surface and thinner walls at the base, attached to a 0.7 mm thick facesheet. The outputs from this research can provide a new route to the design and manufacture of mould tools, which could have significant impacts in the composites sector with new, lighter, more energy efficient tooling.

Keywords Additive manufacturing · Composite tooling · Lattice structures · Heating rate · Thermal efficiency

1 Introduction

The use of additive manufacturing (AM) technologies is growing considerably across different industrial sectors. The freedoms afforded by this layer-wise manufacturing approach open up increasing levels of part complexity as can be seen in, for example, medical devices [1–3], heat exchangers [4–7], and aerospace parts and tooling [8–10]. Moreover, waste is significantly reduced as only material that is required is used in the deposition process. For example, the use of AM for part consolidation has been shown to improve the assembly lifespan by over 200% and achieve a 30% material saving [11]. Additionally, life cycle inventory models have shown a potential cumulative emission reduction of up to 200 million tons of CO_2e by adopting AM lightweight aircraft components by 2050 [12]. These uses of AM show great potential to improve manufacturing efficiency and save energy, especially as build volume capabilities continue to increase [13].

Aside from the primary uses of AM technologies, there is also an increasing use of AM components as a secondary means of manufacture. For example, in casting, where AM is used to create moulds for sand, die and investment casting. A recent example for this is 'Enable Casting' [14] who use traditional casting methods but with AM designed and manufactured moulds. This approach means that far greater levels of part complexity can be achieved at near mass manufacturing scale.

AM technologies and processes can be broadly divided into several subcategories [15] with the most prominent and industrially relevant being the class of technology commonly known as powder bed fusion (PBF). This AM technology

✉ James Kratz
   james.kratz@bristol.ac.uk

✉ Vimal Dhokia
   V.Dhokia@bath.ac.uk

   Max D. A. Valentine
   mv349@bath.ac.uk

1   Department of Mechanical Engineering, University of Bath, Bath, UK

2   Bristol Composite Institute, Department of Aerospace Engineering, University of Bristol, Bristol, UK

3   Department of Mechanical Engineering, University of Bristol, Bristol, UK

is being used across sectors, including mould tool technology for injection moulding [16], thermoforming, and high-performance composite manufacture. The latter area is continually evolving and growing [17–19]. The soaring complexity of products, rapidly compressed design timescales, and growing productivity demand present significant opportunities for the composites industry. This, coupled with the need to continually reduce greenhouse emissions in line with the government target of 60% by 2030 and net-zero emissions by 2050, has created considerable interest [20].

Since the 1970s when high-performance composites were first utilised in aerospace applications, the design and manufacture of composite curing equipment and tools have not changed. The vast majority of mould tools are machined from single large billets of metal, typically Invar, stainless steel, or Inconel, with considerable waste in the form of swarf generated [21]. Furthermore, heating and maintaining heat on large monolithic metal sections is energy intensive and can lead to uneven thermal gradients during the curing process [22]. Combined with the relatively low heat transfer efficiency of air convection in ovens and autoclaves, traditional tooling solutions result in large amounts of wasted energy [23].

There are two immediate opportunities for energy savings in the curing process, firstly by reducing the mass of the equipment and tooling and, secondly, by increasing process heat transfer. The current autoclave curing process can account for approximately 15% of the total energy intensity during a typical fibre-reinforced composite part's life cycle [24]. Additionally, in the automotive industry, while replacing metals with lightweight composites reduces the in-use emissions, these energy savings are largely offset by the increased environmental impact of manufacturing carbon fibre-reinforced polymers (CFRP) [25]. Therefore, an immediate increase in performance and reduction of the total embodied energy can be achieved by specifically targeting the design of the mould tool.

A potential method to improve the heat transfer and thermal responsiveness would be through incorporating lightweight structures into the tooling. These structures would create geometric features that have a larger specific stiffness by reducing the overall mass while maintaining the required overall stiffness. Lattice structures have already been incorporated into a variety of applications to increase heat transfer such as heat exchangers [26] and in pipe flow [27]. Metallic foams have also been shown to increase heat transfer rates, especially in higher porosity foams which have been demonstrated to increase convective heat transfer by up to 10 times [28, 29]. Along with greater heat transfer rates, overall thermal responsiveness of tooling is driven by significant reductions in tool mass that can be achieved through AM methods. The efficacy of lightweight lattice structures on increasing heat transfer performance [30]

therefore highlights the potential of L-PBF to manufacture thermally responsive tooling.

There is a growing use of AM to produce different types of tooling for moulding and curing of different materials [31–39]. The majority of the existing examples employ polymer AM technologies such as fused deposition modelling (FDM) for manufacturing the tooling [18, 40–44]. At the Oak Ridge National Laboratory, a Metal Big Area Additive Manufacturing system has been trialled that uses a low-cost steel wire to manufacture large to near-net shape mould tools [17, 19]. Near-net shape components require either considerable post-processing, or additional treatments in the form of surface coatings. The geometrical features are currently limited to 2.5D planar features. To gain further customisation and higher quality composite parts, an additional method of using carbon fibre filled ABS thermoplastic as the mould tool with a surface coating was trialled to showcase the feasibility of the tools [45]. The large CFRP components were successfully cured in an autoclave at 180°C at a pressure of 620 kPa [46], however, there is still limited research on the use of any fully metallic AM tooling.

Good composite tooling can be characterised by its cost, process efficiency, shape accuracy, thermal capacity and specific stiffness, lifespan, and maximum service temperature, among many other variables [21]. Many of which are difficult characteristics to achieve with polymer based tooling. However, the use of metals rather than polymers allows the tooling to achieve higher service temperatures, greater specific stiffness, and more durable tooling with longer lifespans. Laser powder bed fusion (L-PBF) processes have high feature resolution and low surface roughness and can therefore open the possibility of creating durable, bespoke, and complex designs for lightweight tools not only to withstand the manufacturing cycles but also to provide additional functionalities such as integrated cooling channels and sensors. While the use of L-PBF methods may be able to achieve the desired tooling characteristics, there is currently limited design for manufacture workflows for effective single iteration design of complex manufacturable tooling optimised for energy efficiency making the design of AM cure tools difficult to realise.
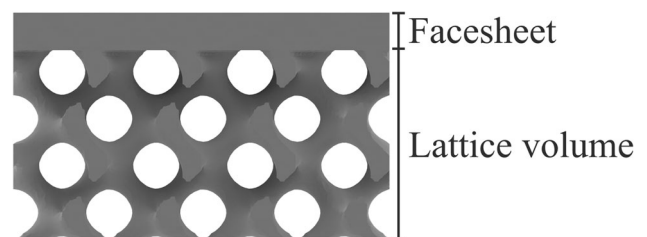

Fig. 1 Sample proposed tooling side profile

In this study the design and manufacture of a new type of AM composite mould cure tool integrating lattice features are explored. The paper is structured into the following sections, first the design guidelines and framework of the tool manufacture is outlined. This is followed by the experimental method including AM build properties, composite curing methodologies, and simulation methods for assessing the physical properties of the tools and lattices. The as-built surfaces of the L-PBF tools will be tested through thermal and pressurised loading of the oven curing process. Finally, the tool performance is assessed based on the geometrical accuracy, thermal properties, and stiffness relative to each other and equivalent monolithic tool designs. The UK has identified the need to develop the capability to digitally design and deliver future composite products as a priority [47], highlighting its importance on a global scale. The outcomes of this study aim to form the basis to radically shorten the design to manufacture time and reduce the environmental impact of complex tooling, targeting single iteration design.

2 Tool design

2.1 Design specification

The selected composite geometry was not the critical feature as the focus of this study is on testing a range of tool geometry variables to gain an understanding of how to design an AM tool. The ideal tool would consist of an infinitely thin, rigid, smooth, and perfectly flat, facesheet to maximise thermal responsiveness and meet dimensional accuracy requirements. The design aim is to maximise each of these qualities in the final tooling. Therefore, a small, simple geometry was selected to manufacture a large number of tools on each AM build plate, maximising the testing capacity. The chosen tool geometry was a 100 mm × 100 mm surface with a solid facesheet and a lattice to stiffen the tool. Stainless steel 316L was used to manufacture the tools. The minimum facesheet surface thickness was approximately 0.7 mm as this is approaching manufacturing limits and meets the
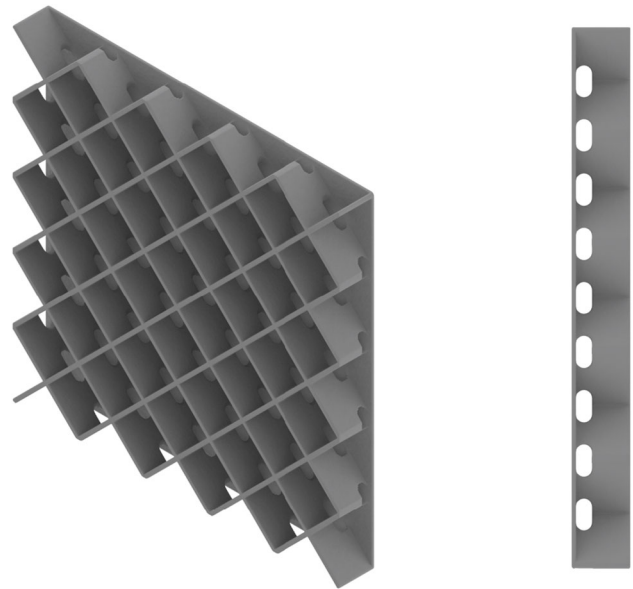

Fig. 3 Modifications to the standard planar diamond lattice structure to promote airflow through the lattice volume

surface bending moment requirements for a flat plate of this size (Fig. 1).

Lattices are structures of repeating geometries that can be defined by a unit cell. The unit cell of a lattice is the smallest repeated unit or geometry that is combined to form the global structure. They are a useful tool in design as they can provide structural advantages, improvements to heat transfer and energy absorption. An advantage of AM is its ability to manufacture complex geometries like lattice structures that are not manufacturable through conventional subtractive techniques. As the reliability and quality of AM components continue to increase, it will be possible to design and manufacture further lattice structures with even smaller unit cell sizes and lower volume fraction percentages (i.e. lower densities). Four lattice unit cell geometries were selected to stiffen the thin facesheet: gyroid, dual-wall gyroid, planar diamond, and a stochastic lattice (Fig. 2).
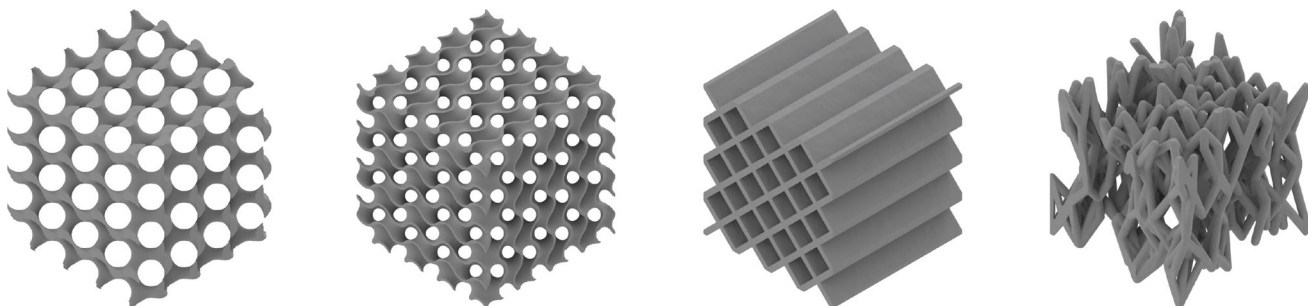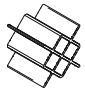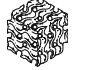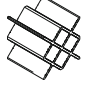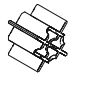

Fig. 2 Lattices of the repeated gyroid, dual-wall gyroid, planar diamond, and stochastic unit cells (in order left-right)

Table 1 Summary of tools and lattice geometry unit cells

ID	Lattice Geometry	Lattice Density (%)	Facesheet Thickness (mm)	Unit Cell
D.26.2	Planar Diamond	26	2	
D.40.1	Planar Diamond	40	1	
D.40.2	Planar Diamond	40	2	
G.26.1	Gyroid	26	1	
G.26.2	Gyroid	26	2	
G.46.1	Gyroid	46	1	
G.46.2	Gyroid	46	2	
DG.46.2	D-Gyroid	46	2	
STk.46.1	Stochastic	46 (Thick strut)	1	
STk.46.2	Stochastic	46 (Thick strut)	2	
STk.24.1	Stochastic	24 (Thick strut)	1	
STk.24.2	Stochastic	24 (Thick strut)	2	
STn.20.1	Stochastic	20 (Thin strut)	1	
STn.20.2	Stochastic	20 (Thin strut)	2	
D.10.075.10	Planar Diamond	10 (x10)	0.75	
D.15.075.10	Planar Diamond	15 (x10)	0.75	
D.10.075.8	Planar Diamond	10 (x8)	0.75	
D.15.075.8	Planar Diamond	15 (x8)	0.75	
D.5.075.5	Planar Diamond	5 (x5)	0.75	
D.10.075.5	Planar Diamond	10 (x5)	0.75	
D.15.075.5	Planar Diamond	15 (x5)	0.75	
D.15(vd2).075.5	Planar Diamond	15 (x5)	0.75	
D.15(vd3).075.5	Planar Diamond	15 (x5)	0.75	
G.10.075.3	Gyroid	10 (x3)	0.75	
G.15.075.3	Gyroid	15 (x3)	0.75	
G.7.075.2	Gyroid	7 (x2)	0.75	
G.10.075.2	Gyroid	10 (x2)	0.75	
G.15.075.2	Gyroid	15 (x2)	0.75	
G.15(25-5).075.2	Gyroid	15 (x2)	0.75	
G.15(25-5).075.3	Gyroid	15 (x3)	0.75	

Gyroid and dual-wall gyroid unit cells are a classification of triply periodic minimal surface (TPMS) geometries, which are defined as lattices that have no joints or discontinuities. These geometries have inherently large surface areas relative to their overall volume and have high specific stiffness.

Due to these properties, TPMS lattices such as the gyroid are commonly used in applications where lightweight components are required [48, 49]. They are found in AM heat exchangers and heat sinks [50, 51], as well as in mechanical and acoustic damping applications [52, 53]. For this

composite layup and cure tools, the specific stiffness potential of both forms of gyroid lattice lend themselves to potentially benefit the structural properties of the tool while increasing surface area for improved convective heat transfer.

Next, stochastic lattices are structures that are randomly generated and can be achieved using algorithms such as voronoi tessellation [54], or other pseudo-random techniques [55]. These lattices have irregular cell geometries and allow for variable struts or random point generation to define the overall geometery [56]. The use of a stochastic lattice brings benefits such as high specific stiffness, shear and impact resistance, desirable damping properties, thermal stability, and good biocompatibility [57]. The overall stiffness of stochastic lattices has been found to be higher than that of a similar volume density isotropic lattice [54] and are therefore particularly applicable in medical implants [58, 59] and other mechanical components that require a high specific stiffness [55]. However, generating stochastic lattices with specific desired mechanical properties can be difficult due to issues relating to manufacturability and the large file size characteristic of irregular geometries as .STL files. The aim of using a stochastic lattice in this application is to maintain the stiffness of the tool while taking advantage of the randomness of the structure by introducing additional turbulence to the airflow behind the tool surface, thereby increasing potential heat transfer through the part [60].

The final lattice geometry investigated was a planar diamond lattice, a simple geometry that adds the required stiffness. Issues with using a planar lattice in an autoclave, however, include a reduced airflow through the underside of the tool. One method of mitigating this is to include cutouts in the walls to promote some airflow within the circulation of the oven for more even heating across the full surface (Fig. 3). The diamond geometry was selected over a honeycomb-style geometry as the 45° angle ensures it can be manufactured by L-PBF without need for support structures or unit cell size constraints to preserve the surface quality throughout the build volume. The inherent simplicity of the planar lattice also enables the flexibility to include graded density lattices [61], spatially irregular planar lattices [62], or hierarchical planar lattices [63] to optimise the lattice mechanical properties. These features were all created by implicit modelling software, Gen3D [64, 65].

The flat plate tool geometries consist of variations on these four lattice geometries. Each tool sample had modifications to the lattice density, unit cell size or strut thickness, along with the facesheet thickness and lattice type specified above. Further to the four lattice geometries, specific variations on the gyroid and planar diamond geometries were specified. Two variations of graded gyroid lattices were tested with a 5% volume fraction density at the base and 25% density at

the tool surface to add mass closer to the tool surface, increasing the stiffness in this region and promoting convective heat transfer throughout the cure cycle. Two variations of the planar diamond lattice had 2 to 3 mm cutouts at the corners of the diamonds to promote airflow between the unit cells. The final tool lattice geometry specifications are summarised in Table 1, and the nomenclature for the tool name references is described below:

$$\underbrace{G}_{\text{Unit cell}} \cdot \underbrace{10}_{\text{Density}} \cdot \underbrace{075}_{\text{Facesheet thickness}} \cdot (\underbrace{3}_{\text{# unit cells}})$$
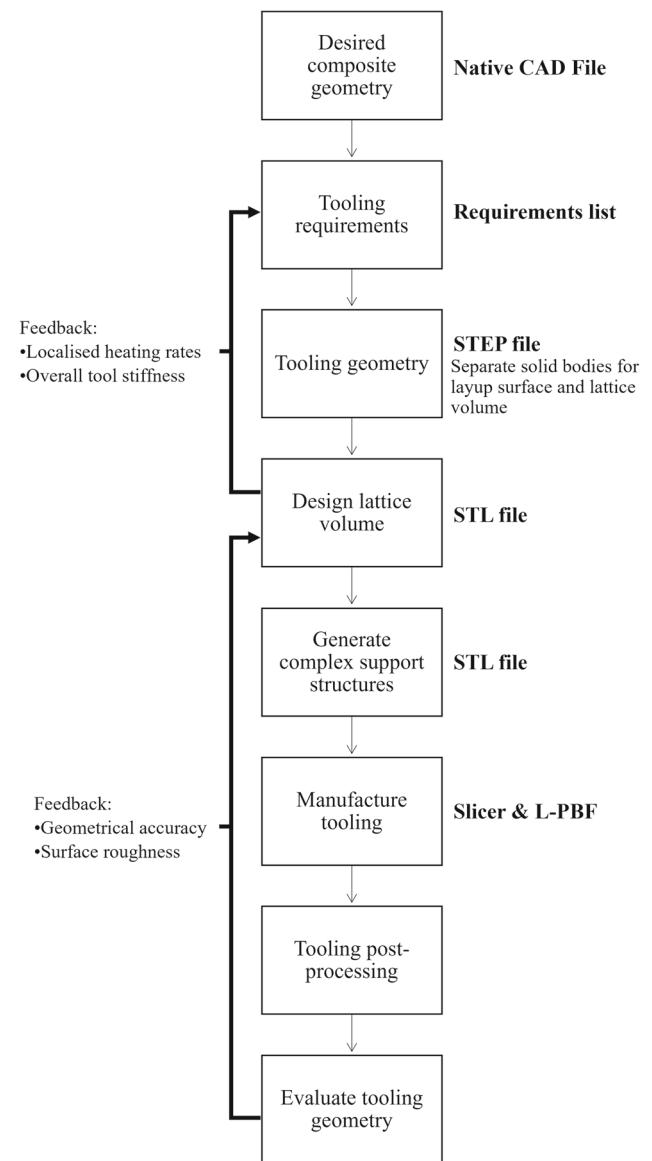

Fig. 4 Proposed DfAM framework for designing tailored AM composite tooling

Table 2 Renishaw AM250 build parameters

Parameter	Value	Unit
Powder Size	10–40	μm
Laser Power	200	W
Exposure Time	80	μs
Point Distance	60	μm
Hatch Spacing	110	μm
Layer Height	50	μm

2.2 Design framework

Figure 4 outlines the framework for the design for AM (DfAM) workflow to create unique tailored AM composite tooling. The work in this research serves to help provide the necessary information to design the lattice volumes and facesheets by understanding how different geometries behave in this application.

3 Experimental method

3.1 Tool manufacturing

The metal tools were manufactured out of 316L Stainless Steel (SS316L) powder using a Renishaw AM250 L-PBF machine. SS316L was selected due to its similar properties to tool steel and its ease of manufacture through L-PBF AM. Additional build process parameters are summarised in Table 2. Two full build plates were required for all tools and the build plate and process parameters were kept consistent across both builds. The tools were oriented on their side with the facesheet facing slightly offset from the $y-z$ plane to enhance powder spreading, reduce damage to the wiper blade, and fit up to 16 tools on each build plate (Fig. 5).

Before laying up the composite pre-preg laminates, light grit sandpaper removed any partially sintered powder particles from the facesheet and the tools were cleaned thoroughly to ensure no remaining powder was present on the part. There was no additional post-processing of the tools after removing the support structures from the bottom surface. Keeping a close-to as-built surface on the AM tools limits the cost and time to manufacture each of the tools and enables a preliminary assessment of AM tooling.

The geometrical accuracy of the tools was evaluated to ensure flatness. Once removed from the build plate, the top surface of each tool was scanned using a 7-axis Romer Absolute Arm 7535 SE by Hexagon Meteorology and CMS108Ap laser scanner. The post-processing of the resulting point
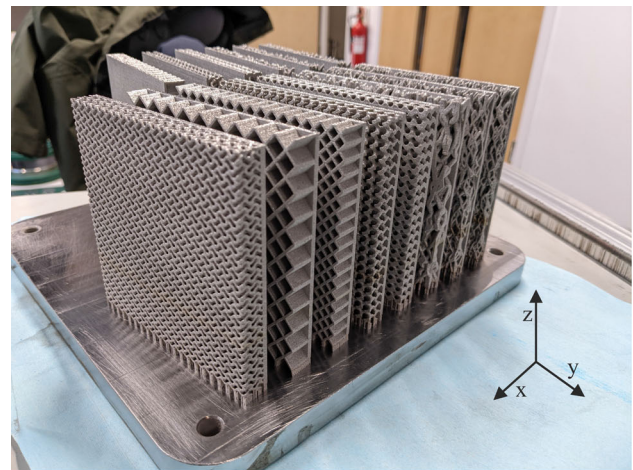
(a) AM Build 1 (14 Tools)
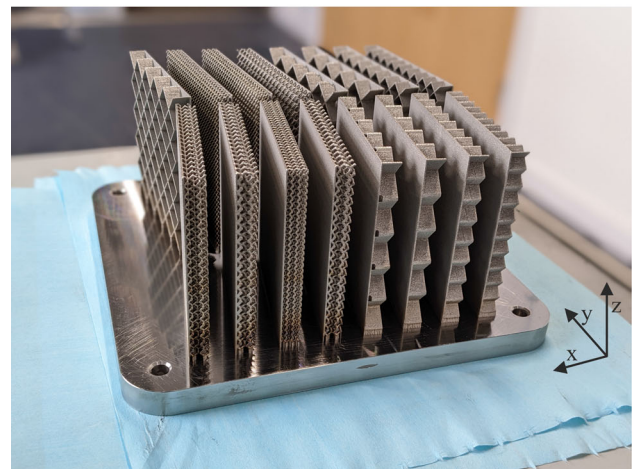

(b) AM Build 2 (16 Tools)

Fig. 5 AM Build of all 30 tools: (a) AM Build 1 (14 Tools); (b) AM Build 2 (16 Tools)

clouds was performed in MATLAB [66]. After applying a transformation matrix to orient each point cloud data to the origin, level with the X-Y plane, an average surface was calculated. The reported flatness values were calculated by the distance magnitude of each point in the point cloud from the average surface, and the top 5% of peak values were taken as the surface deviation.

3.2 Composite material and manufacturing

A pre-impregnated (pre-preg) material comprising of a twill weave fabric formed of T700 carbon fibre as reinforcement in a toughened matrix of SHD MTC400 epoxy resin was used (MTC400-C415T-T700-12K-38%RW-1250). The

Fig. 6 Schematic of bagging scheme including daisy-chain connection of AM tools


3.3 Physical data processing
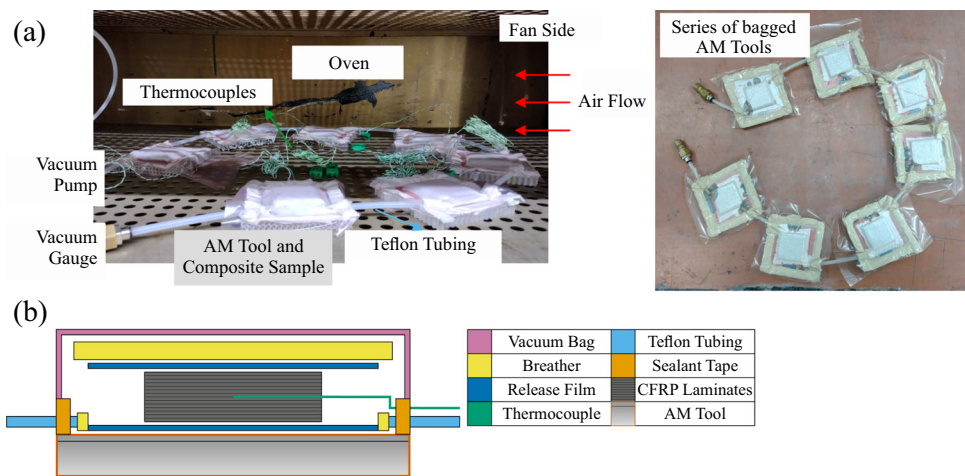
composite laminate was prepared using fourteen plies of 40 mm x 40 mm pre-preg to form a theoretical cured part thickness of 7 mm. A thermocouple was placed within the f stack between the seventh and eighth plies to capture the thermal history during the curing process. A standard composite vacuum bagging scheme, as shown in Fig. 6, was used to prepare the composite on the AM tools. PTFE tubes were used to daisy-chain a series of 7 or 8 tools together to reduce the total number of curing cycles under the restriction of a single vacuum pump. The bag quality was checked to ensure it could achieve a vacuum pressure of up to 100 kPa.

The prepared tools were then placed in a conventional oven (Carbolite) for curing. The thermocouples were connected to a datalogger (Pico Logger), and temperature data were collected at a sampling rate of 1 Hz. The composite parts were then cured according to the fastest cure schedule suggested by the supplier. The cure schedule was 3 °C / min to 135 °C, dwell for 1 h for full cure, and followed by a cool down set at 2 °C / min to 30 °C.

The thermal responsiveness of the tools was evaluated both through the heating rate of the tool relative to the oven, as specified in Section 3.2, and by the overshoot temperature. The heating rate and overshoot for the different tool geometries were calculated from the thermocouple data (Fig. 7). Firstly, the heating rate was calculated from the initial region of 1000 to 2000 s in each tool's thermal profile, as this region is solely a function of the tool and oven, and it is after the heating reaches a steady state. The linear trend implies there is no chemical reaction occurring in the polymer and therefore is dominated by the heat transfer rather than the exothermic reaction. The thermal overshoot was calculated as the difference between the peak temperature and the set temperature of the oven. The curing of epoxy is an exothermic reaction and if the heating rate is fast and heat transfer rates through the oven are low enough, it can lead to excess energy generation during the process, causing the temperatures to exceed the oven temperature. This overshoot temperature can

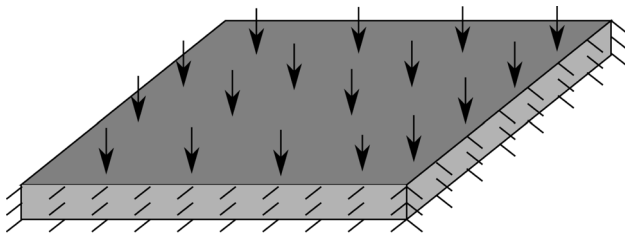**Fig. 7** Sample temperature history of one tool during the oven curing process
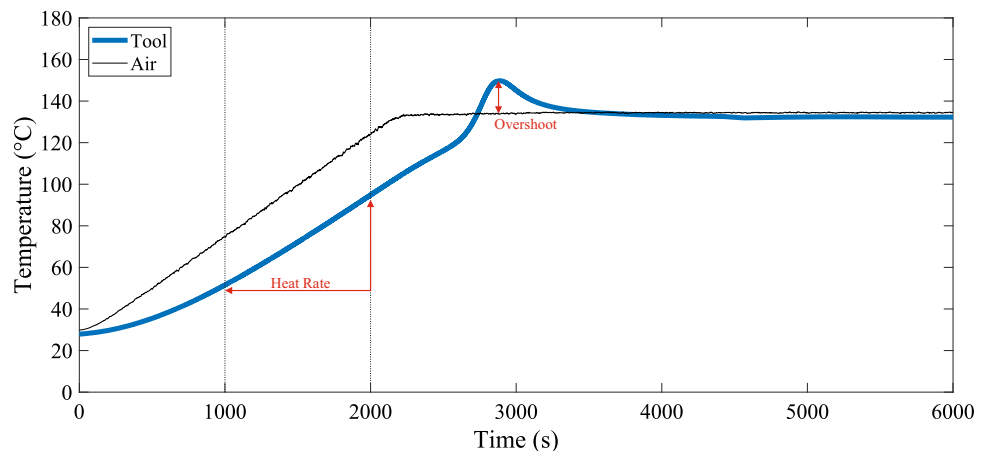
Fig. 8 Each plate was clamped around all four side faces and a uniform pressure (P) of 0.1 MPa applied to the upper solid (non-lattice) face

indicate the thermal response of the tool as it will relate both to the heat transfer into the composite part and how effective the tool is at controlling the thermal overshoot. Each of these metrics was compared against each other, along with the simulated tool stiffness, in order to determine which of the tools had the greatest potential for more complex composite geometries.

3.4 Tool stiffness modelling

Three dimensional volume meshes were created from the STL files using Simpleware ScanIP software [67]. The resampling function was used to define the size of the voxels, and this was set to 0.5 mm cubes. The STL was then converted to a voxel mask prior to meshing within the software; this procedure enabled the software to mesh the part without being influenced by the pre-existing STL surface mesh and could be applied consistently to all lattices. Tetrahedral meshes were created within the software with a range of densities. The resultant mesh quality metrics are summarised in the supplementary material.
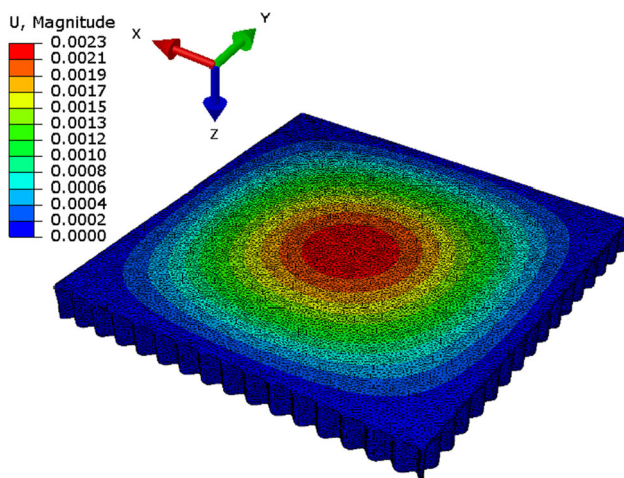

Fig. 9 Typical contour plot of the simulation results, the lattice shown is a Diamond lattice of 40% volume fraction. Displacement magnitude in mm
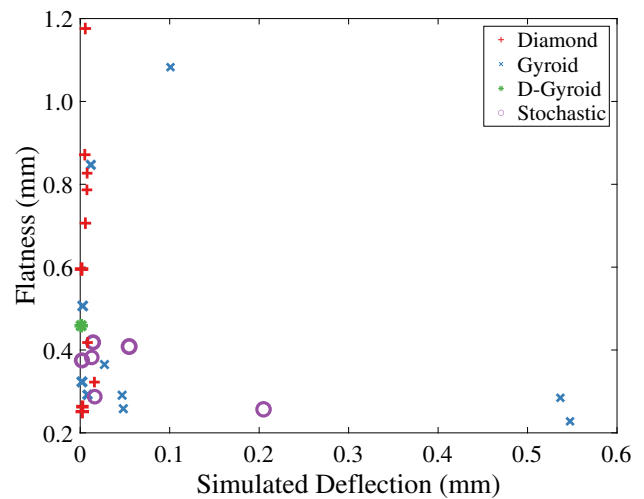

Fig. 10 Simulated tool stiffness relative to the manufactured tool flatness

The tool stiffness was quantified with finite element modelling using ABAQUS software with the implicit static solver [68]. Quadratic tetrahedral elements were used (C3D10) and assigned linear elastic properties of steel (E=200 GPa, v=0.3). A pressure load of 0.1 MPa was applied to the upper tool surface and the four side edges were clamped in all degrees of freedom (Fig. 8). The magnitude of lateral deflection of the tool was calculated and a contour plot of a typical model is shown in Fig. 9. A mesh convergence study was performed using the dual-walled gyroid lattice model (Figure A1) and the maximum displacement values converged at 1.22 million elements with a mean element edge length of 0.83 mm. The plate deflection values were also compared to
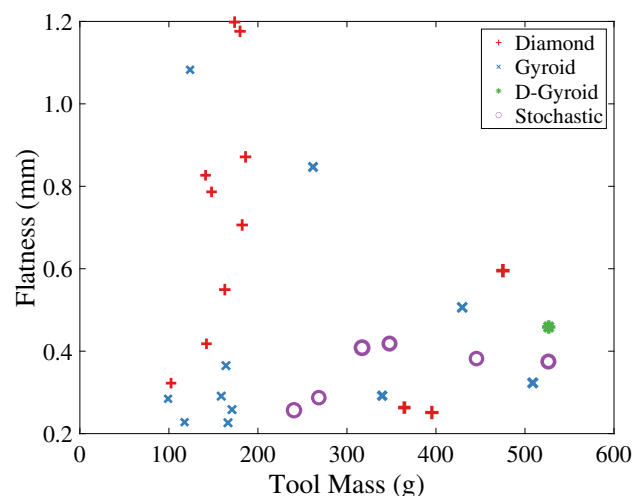

Fig. 11 Tool surface flatness from overall tool mass

that of solid square plates of (a) equivalent thickness, and (b) equivalent volume, and the data found for each lattice as a relative deflection where:

$$\text{Relative deflection} = \frac{\text{Lattice deflection}}{\text{Equivalent solid deflection}}$$

4 Results

4.1 Geometrical accuracy

Small degrees of thermal deformation occurred during manufacturing as a result of the thermal gradient in the AM build chamber, as evidenced by a slight bowing pattern across $\approx 80\%$ of the tools. Despite the lack of post-processing or heat treatment to relieve this residual stress, the magnitude of deformation was less than 1 mm across a majority of the tools. Only the D.15.075.8, D.15(vd2).075.5, and G.10.075.2 tools had total deviations greater than 1 mm. While the lower stiffness relative to a solid monolithic tool could lead to the thermal deformation, there was no significant relationship found between the simulated tool stiffness (Fig. 10) and the geometrical accuracy of the tools. However, Fig. 11 shows the relationship between the tool mass and facesheet flatness. Although the relationship was not directly proportional, it can be seen that the lower mass tools lead to worse degrees of flatness, implying there is less support from the lattice and less bulk mass. However, flat and lightweight tools are possible. Further relationships between the other three design variables and the tool flatness can be found in Supplementary Section B.
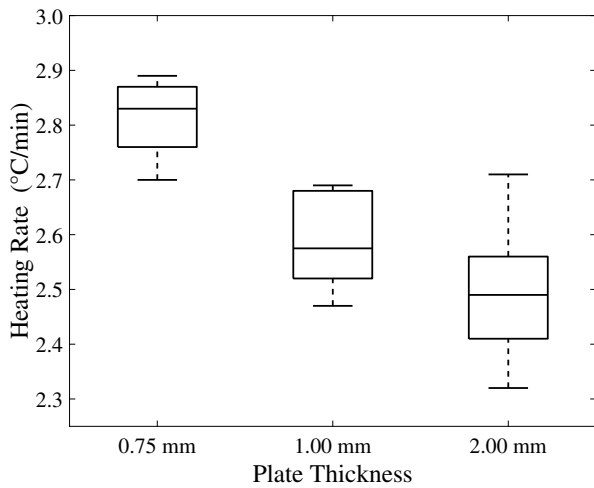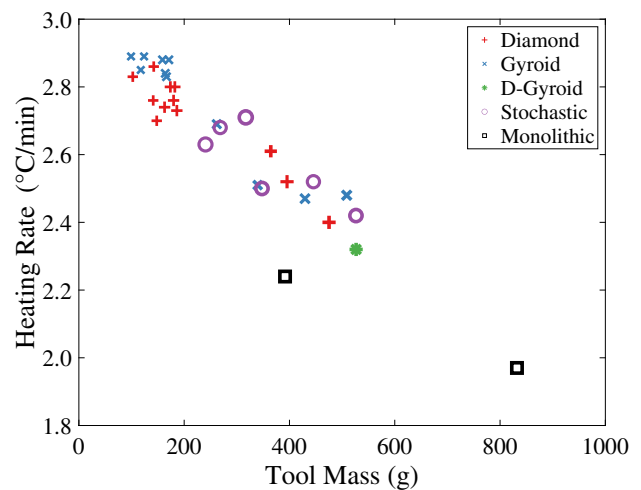

(a) Composite heating rate from facesheet thickness.
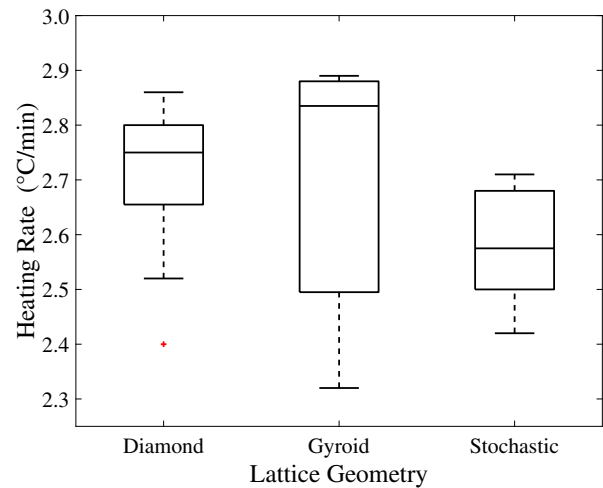
(b) Composite heating rate from lattice geometries.
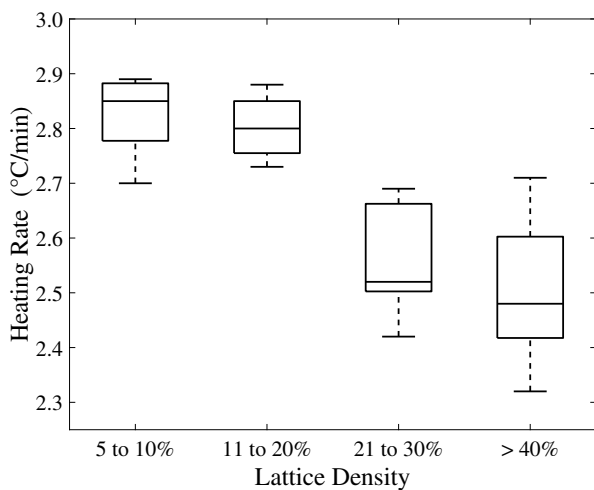
(c) Composite heating rate from lattice density.

(d) Composite heating rate from overall tool mass.

Fig. 12 Heating rate during cure cycle of all thirty tools: (a) Composite heating rate from facesheet thickness; (b) Composite heating rate from lattice geometries; (c) Composite heating rate from lattice density; (d) Composite heating rate from overall tool mass

4.2 Thermal responsiveness

Figures 12 and 13 both show a summary of the thermocouple results in terms of the measured heating rate and overshoot temperatures. Initial trends show that the mass of the tools was directly proportional to both the heating rate (Fig. 12d) and the overshoot temperature (Fig. 13d). However, the trend for the overshoot temperature was not uniform as the 0.75 mm thick plate with gyroid lattices deviated from the linear trend. Specifically, the tools with the graded lattice in the z direction of the tool showed this response. The combination of the increased tool mass near the faceplate with greater void fraction at the bottom of the tool lattice volume was beneficial. The low lattice density at the base led to additional airflow through the lattice volume and the added material near the

faceplate helped to reduce the magnitude of the exotherm by acting as a heat sink. Compared to 5 mm and 10 mm thick monolithic tools, the tools investigated in this research were able to achieve faster heating rates with similar tool mass (Fig. 12d). The monolithic tools were able to reduce the magnitude of overshoot (Fig. 13d) as a result of the lower heating rates. This trend was consistent with all thirty tools and the two monolithic tools, as shown by Fig. 14.

The plate thickness can be seen to have had a significant impact on both the tool heating rate (Fig. 12a) and thermal overshoot (Fig. 13a). The thinner plates allowed for a faster heating rate as there was less material for the environment to heat up before it could cure the composite epoxy. This was seen to have a significant difference ($p < 0.001$) when comparing the 0.75 mm plates with both the 1.00 mm and
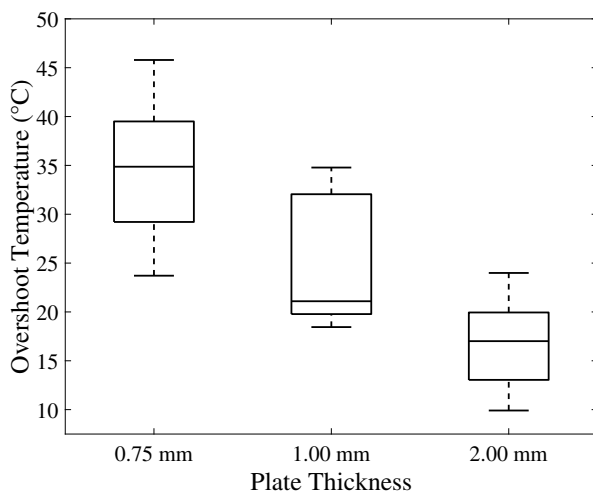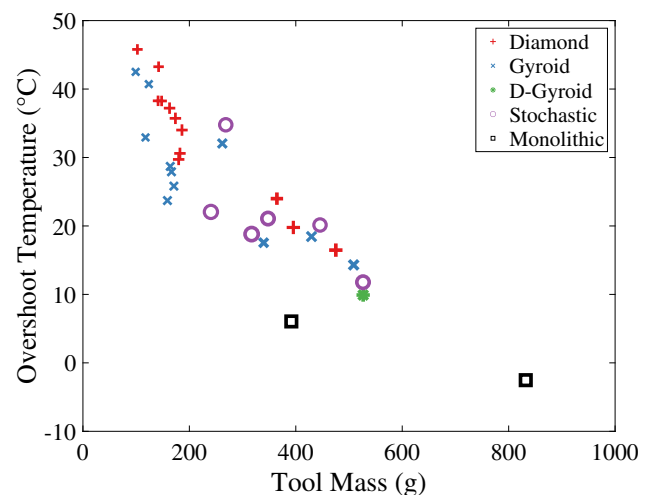

(a) Thermal overshoot from facesheet thickness.
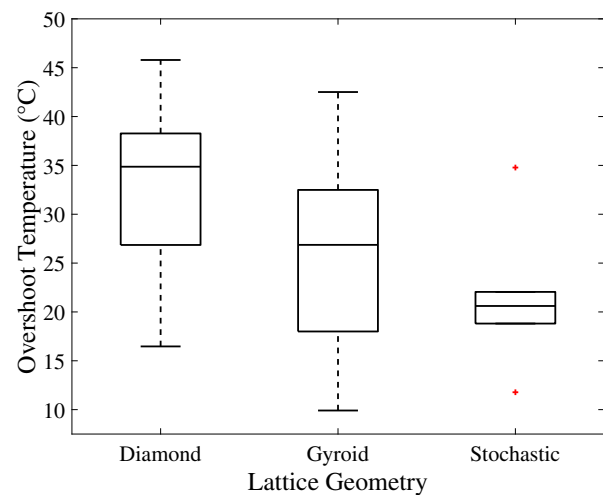
(b) Thermal overshoot from lattice geometries.
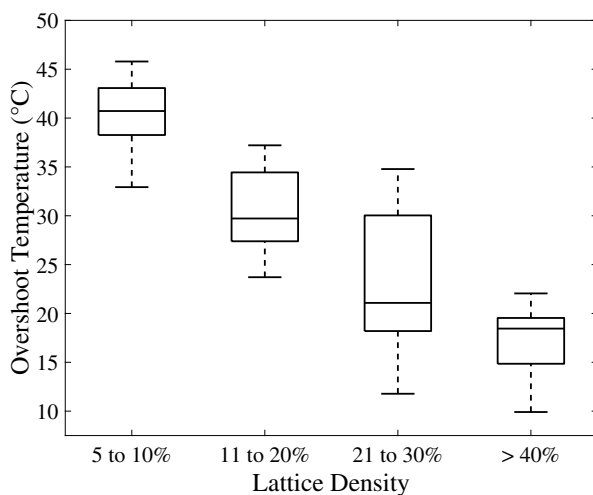
(c) Thermal overshoot from lattice density.

(d) Thermal overshoot from overall tool mass.

Fig. 13 Thermal overshoot during curing of all thirty tools: (a) Thermal overshoot from facesheet thickness; (b) Thermal overshoot from lattice geometries; (c) Thermal overshoot from lattice density; (d) Thermal overshoot from overall tool mass
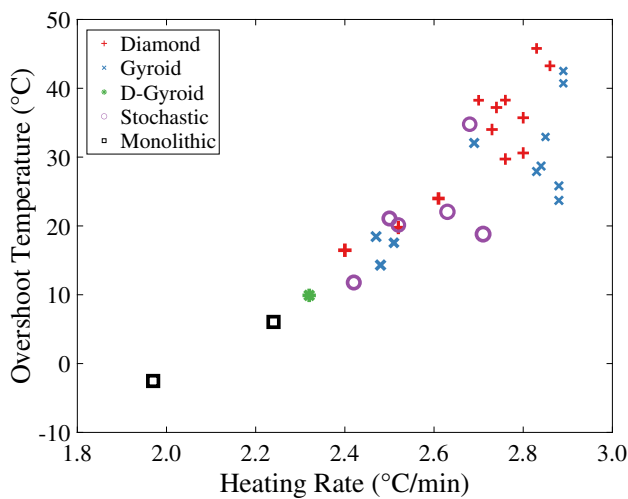
Fig. 14 Relationship between thermal overshoot and heating rate

Fig. 15 Scatterplot of the thickness of an equally stiff monolithic plate against the relative deflection of an equivalent thickness solid plate

2.00 mm plates, but not between these two thicker plates. However, the effect of the difference between the 1.00 mm and 2.00 mm plates could have been reduced due to the larger lattice densities used in these tool samples, therefore reducing the individual impact of the plate thickness. Similarly the significance of the plate thickness on thermal overshoot was significant between the 0.75 mm plates with both the 1.00 mm ($p < 0.01$) and 2.00 mm plates ($p < 0.001$), but not between the two thicker plates. The tools with slower heating rates and therefore greater thermal mass were able to mitigate the overshoot effect, leading to smaller overshoot temperatures on the thicker and heavier tools.

There was no specific dependence towards the tool heating rate (Fig. 12b) or overshoot (Fig. 13b) with respect to the overall lattice structure geometries selected.

Figures 12c and 13c both show the relationships of the lattice density with the heating rate and thermal overshoot respectively. As the density of the lattice was directly linked to the overall tool mass, the results were fittingly similar to the relationships discussed above. The heating rate showed a significant dependence on the lattice density when comparing the set lighter than 20% with the set greater than 20% ($p < 0.001$). The thermal overshoot did show a significant difference between the lowest density range, $\leq 10\%$, and the range from 11 to 20% ($p < 0.01$). This indicates that the overshoot appears to be proportional to lattice density, regardless of the facesheet thickness, while the heating rate was more sensitive to the facesheet thickness.

4.3 Tool stiffness

Figure 15 shows that the stochastic lattice supported facesheet tools had the lowest stiffness, with one lattice demonstrating over 650 times the deflection of a solid plate of equivalent thickness (baed on the tool facesheet thickness). All of the
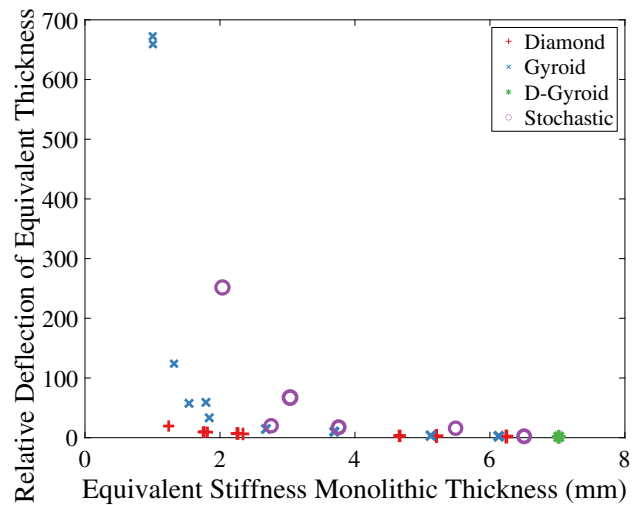
lattices had greater deflection magnitudes than the equivalent thickness solid plate. For a given volume and thickness, as the mass is removed, the effective bending stiffness would reduce. This is why the D-Gyroid has the stiffness closest to a solid plate, as it had the greatest mass of all manufactured tools.

When the relative deflection to an equivalent volume tool (based on a solid tool equal to the total tool volume) was assessed, the lattice deflections were similar to the solid plates (Fig. 16), demonstrating the importance of lattice density to the tool stiffness behaviour. However, the lattice structure was also influential; while the majority of the lattice structures had a smaller deflection as compared to an equivalent volume solid plate, some of the stochastic lattices had over twice the
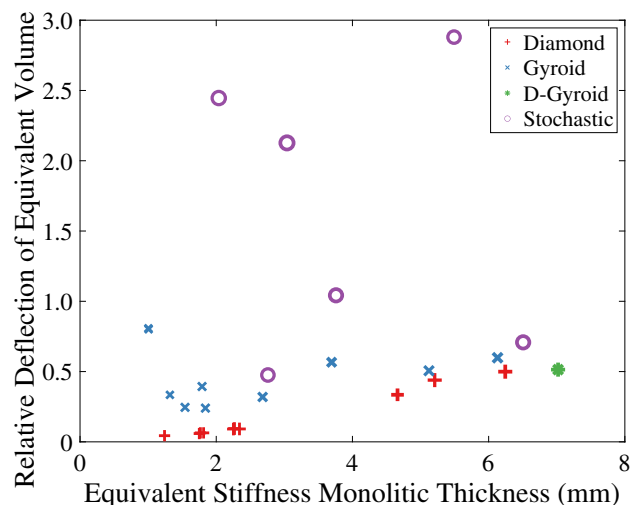

Fig. 16 Scatterplot of the thickness of an equally stiff monolithic plate against the relative deflection of an equivalent volume solid plate

deflection. Conversely the diamond lattices had the lowest relative deflection.

The magnitude of relative deflection of the equivalent volume tool is much lower than the equivalent thickness tools indicating that the lattice geometry and density design decisions have a large impact on the overall tool stiffness.

5 Discussion

As a result of testing these variables for composite curing on an initial geometry with minimal post-processing, the following was determined: Firstly, the cure tools were all able to withstand the force of the vacuum and thermal load, while maintaining vacuum integrity. As each tool had limited post-processing treatment (to help improve the surface quality of the facesheet) it was important to ensure the as-built surface was able to hold a vacuum using conventional bagging techniques. Secondly, the lattices showed promise both as a mass reduction method and as a means of regulating the thermal properties. With regards to the mass reduction, while maintaining a constant tool volume each sample had sufficient stiffness to be used in a small case study, however, simulations showed that the monolithic equivalent was stiffer than each AM tool counterpart. Therefore, the lattice geometry, density, and the overall tool stiffness should be accounted for in the design stage. The thermal properties of each tool were improved relative to the equivalent size monolithic tool as the AM tools on average had faster heating rates and the airflow around the tool and part regulated the overshoot and enabled a controlled cooling rate. Additionally, the ability to select a specific lattice geometry for a desired thermal performance across a larger tool geometry with increased complexity provides an exciting opportunity to further take advantage of using AM to design and manufacture composite mould tools.

Evaluating the lattice geometries and respective plate thickness that demonstrate the most promise was achieved by optimising the tool heating rate relative to its geometrical accuracy as the two determining factors. Figure 17 shows the relationship of these two variables, where the optimum response in the bottom right corner indicates tools that had a high heating rate and high degree of geometrical accuracy. It shows that typically the tools with low mass had better performance due to the heating rate being close to 3°C/min as a result of the thin facesheet and lower lattice density. The gyroid lattice based tools exhibited high heating rates while maintaining low surface deviations, leading to the best tool performance. Specifically, the graded gyroid lattices had the best overall performance in terms of specific stiffness, geometrical accuracy, and thermal response (Fig. 17).

While the results obtained in the present study show improvements relative to monolithic tools on a small scale,
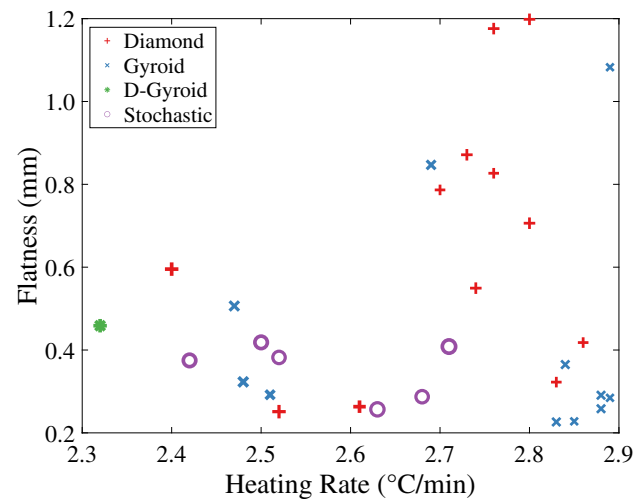

Fig. 17 Top tool optimisation. Marker size is proportional to lattice density and line thickness is proportional to the facesheet thickness

further investigation applying these design techniques to larger and more complex shape composite tools is needed to increase the technology readiness level. As the tools were tested in an as-built state, the facesheet surface roughness would be considered too poor for certain applications. However, this can be addressed through post-processing methods such as machining the facesheet where the composite will be in direct contact during the curing stage. Additionally, as the quality of future AM and L-PBF technologies improves, the need for post-machining of the facesheet to improve surface roughness will be reduced. Studies that investigate the optimisation of surface roughness through laser scanning and build strategies have been shown to achieve $R_a \approx 9\mu m$ for copper alloys [69], $R_a \approx 4\mu m$ and lower for AlSi10Mg [70], and a reduction of the surface roughness by more than $R_a = 10\mu m$ down to $R_a \approx 20\mu m$ using SS316L [70]. Future work will focus on investigating the specific properties and optimisation of the lattice structures, post-processing of the tool and facesheet surfaces, and methods for scaling up the output part size.

6 Conclusion

This investigation demonstrates the potential for using additive manufacturing as a method for producing a new type of composite tooling. Advantages were gained in (1) better thermal responsiveness, (2) ability to deal with the curing exotherm in a more controlled manner, and (3) enhanced design flexibility to enable tool geometry optimisation to achieve the desired tool properties and accuracy. Thermal performance of the graded gyroid lattice based tools was able to achieve above 93% of the applied heating rate in an oven cure cycle. These lightweight tools had the equiv-

alent stiffness of a monolithic tool over $2.5\times$ the thickness of the facesheet. Higher density lattice structures achieved an equivalent tool stiffness of a monolithic tool up to $3.5\times$ the facesheet thickness (i.e. a 2 mm AM tool had the equivalent stiffness of a 7 mm monolithic tool). Using the lattice geometries, the tools achieved a heating rate increase of up to 17%, when compared to monolithic equivalents of a similar mass. Comparing the effects of geometrical variables of the tools, the results showed that the thermal overshoot has a stronger relationship with the lattice density (Fig. 13c), whereas the heating rate was more sensitive to the facesheet thickness (Fig. 12a). Out of the thirty tools tested, the graded gyroid lattice supported plates were the two most promising lattice geometries as they promoted airflow below the facesheet while maintaining the desired thermal mass and stiffness where required. The use of AM presents a new opportunity for a paradigm shift in the composite tooling industry. The outcomes from this research demonstrate an original approach to developing a new type of mould tool, which can have significant impacts in the composites sector.

Supplementary Information The online version contains supplementary material available at https://doi.org/10.1007/s00170-023-11254-y.

Declarations

Competing Interests The authors declare no competing interests.

References

1. Li C, Pisignano D, Zhao Y et al (2020) Advances in medical applications of additive manufacturing. Engineering 6(11):1222–1231. https://doi.org/10.1016/j.eng.2020.02.018
2. Salmi M (2021) Additive manufacturing processes in medical applications. Materials 14(1):1–16. https://doi.org/10.3390/ma14010191
3. Patel P, Gohil P (2021) Role of additive manufacturing in medical application COVID-19 scenario: India case study. J Manuf Syst 60(November 2020):811–822. https://doi.org/10.1016/j.jmsy.2020.11.006
4. Deisenroth DC, Moradi R, Shooshtari AH et al (2018) Review of heat exchangers enabled by polymer and polymer composite additive manufacturing. Heat Trans Eng 39(19):1652–1668. https://doi.org/10.1080/01457632.2017.1384280
5. Scheithauer U, Schwarzer E, Moritz T et al (2018) Additive manufacturing of ceramic heat exchanger: opportunities and limits of the lithography-based ceramic manufacturing (LCM). J Mater Eng Perform 27(1):14–20. https://doi.org/10.1007/s11665-017-2843-z
6. Tiwari R, Andhare RS, Shooshtari A et al (2019) Development of an additive manufacturing-enabled compact manifold microchannel heat exchanger. Appl Ther Eng 147(April 2018):781–788. https://doi.org/10.1016/j.applthermaleng.2018.10.122
7. Kaur I, Singh P (2021) State-of-the-art in heat exchanger additive manufacturing. Int J Heat Mass Trans 178(121):600. https://doi.org/10.1016/j.ijheatmasstransfer.2021.121600
8. Diegel O, Schutte J, Ferreira A, et al (2020) Design for additive manufacturing process for a lightweight hydraulic manifold. Additive Manufacturing 36(June):101,446. https://doi.org/10.1016/j.addma.2020.101446
9. Blakey-Milner B, Gradl P, Snedden G et al (2021) Metal additive manufacturing in aerospace: a review. Mater Des 209(110):008. https://doi.org/10.1016/j.matdes.2021.110008
10. Khorasani M, Ghasemi AH, Rolfe B et al (2022) Additive manufacturing a powerful tool for the aerospace industry. Rapid Prototyping Journal 28(1):87–100. https://doi.org/10.1108/RPJ-01-2021-0009
11. Yang S, Min W, Ghibaudo J et al (2019) Understanding the sustainability potential of part consolidation design supported by additive manufacturing. J Cleaner Production 232:722–738. https://doi.org/10.1016/j.jclepro.2019.05.380
12. Huang R, Riddle M, Graziano D et al (2016) Energy and emissions saving potential of additive manufacturing: the case of lightweight aircraft components. Journal of Cleaner Production 135:1559–1570. https://doi.org/10.1016/J.JCLEPRO.2015.04.109
13. Hanaphy P (2022) SLM solutions to develop "world's largest" metal 3D printer for the us air force. https://3dprintingindustry.com/news/slm-solutions-to-develop-worlds-largest-metal-3d-printer-for-the-us-air-force-215010/
14. Enable Manufacturing Ltd. (2021) New Vacuum Additive Casting process set to rock the metal 3D printing world. https://enable.parts/2021/05/new-vacuum-additive-casting-process-set-to-rock-the-metal-3d-printing-world
15. British Standards Institution (2022) BS EN ISO/ASTM 52900:2021 - Additive manufacturing - General principles - Fundamentals and vocabulary. Tech. rep, British Standard Institution
16. Papadakis L, Avraam S, Photiou D, et al (2020) Use of a holistic design and manufacturing approach to implement optimized additively manufactured mould inserts for the production of injection-moulded thermoplastics. J Manuf Mater Process 4(4). https://doi.org/10.3390/jmmp4040100

17. Hassen AA, Lindahl J, Springfield R, et al (2016) The durability of large-scale additive manufacturing composite molds. In: CAMX Conference Proceedings, Anaheim, CA, https://www.researchgate.net/publication/324391116

18. Sudbury TZ, Springfield R, Kunc V et al (2017) An assessment of additive manufactured molds for hand-laid fiber reinforced composites. Int J Adv Manuf Technol 90(5–8):1659–1664. https://doi.org/10.1007/s00170-016-9464-9

19. Hassen AA, Noakes M, Nandwana P, et al (2020) Scaling Up metal additive manufacturing process to fabricate molds for composite manufacturing. Additive Manufacturing 32(March 2019):101,093. https://doi.org/10.1016/j.addma.2020.101093

20. Sharma A, Johnson B (2020) UK sets ambitious new climate target ahead of UN Summit. Tech. rep., https://www.gov.uk/government/news/uk-sets-ambitious-new-climate-target-ahead-of-un-summit

21. Li Y, Xiao Y, Yu L, et al (2022) A review on the tooling technologies for composites manufacturing of aerospace structures: materials, structures and processes. Composites Part A: Applied Science and Manufacturing 154(June 2021):106,762. https://doi.org/10.1016/j.compositesa.2021.106762

22. Centea T, Peters G, Hendrie K et al (2017) Effects of thermal gradients on defect formation during the consolidation of partially impregnated prepregs. Journal of Composite Materials 51(28):3987–4003. https://doi.org/10.1177/0021998317733317

23. Mirzaei S, Krishnan K, Al Kobtawy C et al (2021) Heat transfer simulation and improvement of autoclave loading in composites manufacturing. Int J Adv Manuf Technol 112(11–12):2989–3000. https://doi.org/10.1007/s00170-020-06573-3

24. Song YS, Youn JR, Gutowski TG (2009) Life cycle energy analysis of fiber-reinforced composites. Composites Part A: Applied Science and Manufacturing 40(8):1257–1265. https://doi.org/10.1016/j.compositesa.2009.05.020. www.sciencedirect.com/science/article/pii/S1359835X09001687

25. Duflou JR, De Moor J, Verpoest I et al (2009) Environmental impact analysis of composite use in car manufacturing. CIRP Annals 58(1):9–12. https://doi.org/10.1016/j.cirp.2009.03.077. www.sciencedirect.com/science/article/pii/S0007850609000304

26. Lai X, Wang C, Peng D et al (2021) Analysis of heat transfer characteristics of a heat exchanger based on a lattice filling. Coatings 11(9):1–13. https://doi.org/10.3390/coatings11091089

27. Koneri R, Mulye S, Ananthakrishna K et al (2021) Additive manufacturing of lattice structures for heat transfer enhancement in pipe flow. Springer Singapore. https://doi.org/10.1007/978-981-15-5689-0_21

28. Tian Y, Zhao CY (2011) A numerical investigation of heat transfer in phase change materials (PCMs) embedded in porous metals. Energy 36(9):5539–5546. https://doi.org/10.1016/j.energy.2011.07.019

29. Rehman Tu, Ali HM, Janjua MM et al (2019) A critical review on heat transfer augmentation of phase change materials embedded with porous materials/foams. Int J Heat Mass Trans 135:649–673. https://doi.org/10.1016/j.ijheatmasstransfer.2019.02.001

30. Sajjad U, Rehman Tu, Ali M et al (2022) Manufacturing and potential applications of lattice structures in thermal systems: a comprehensive review of recent advances. Int J Heat Mass Trans 198(123):352. https://doi.org/10.1016/j.ijheatmasstransfer.2022.123352

31. King D, Tansey T (2003) Rapid tooling: selective laser sintering injection tooling. J Mater Process Technol 132(1–3):42–48. https://doi.org/10.1016/S0924-0136(02)00257-1

32. Kovács JG, Szabó F, Kovács NK et al (2015) Thermal simulations and measurements for rapid tool inserts in injection molding applications. Appl Ther Eng 85:44–51. https://doi.org/10.1016/j.applthermaleng.2015.03.075

33. Bard J, Cupkova D, Washburn N et al (2018) Robotic concrete surface finishing: a moldless approach to creating thermally tuned surface geometry for architectural building components using Profile-3D-Printing. Construction Robotics 2(1–4):53–65. https://doi.org/10.1007/s41693-018-0014-x

34. Zink B, Kovács NK, Kovács JG (2019) Thermal analysis based method development for novel rapid tooling applications. Int Commun Heat Mass Trans 108(August):104,297. https://doi.org/10.1016/j.icheatmasstransfer.2019.104297

35. Bagalkot A, Pons D, Clucas D et al (2019) A methodology for setting the injection moulding process parameters for polymer rapid tooling inserts. Rapid Prototyping Journal 25(9):1493–1505. https://doi.org/10.1108/RPJ-10-2017-0217

36. Sama SR, Badamo T, Manogharan G (2020) Case studies on integrating 3D sand-printing technology into the production portfolio of a sand-casting foundry. Int J Metalcasting 14(1):12–24. https://doi.org/10.1007/s40962-019-00340-1

37. Yang Y, Li H, Xu Y et al (2019) Fabrication and evaluation of dental fillers using customized molds via 3D printing technology. Int J Pharma 562(December 2018):66–75. https://doi.org/10.1016/j.ijpharm.2019.03.024

38. Seleznev M, Roy-Mayhew JD (2021) Bi-metal composite material for plastic injection molding tooling applications via fused filament fabrication process. Additive Manufacturing 48(PA):102,375. https://doi.org/10.1016/j.addma.2021.102375

39. Kuo CC, Lin BH, Luo ZT (2022) A new hybrid process combining rapid tooling and machining to manufacture an injection mold with micro features. Int J Adv Manuf Technol 119(9–10):6349–6360. https://doi.org/10.1007/s00170-021-08529-7

40. Masood SH, Song WQ (2004) Development of new metal/polymer materials for rapid tooling using Fused deposition modelling. Materials and Design 25(7):587–594. https://doi.org/10.1016/j.matdes.2004.02.009

41. Lušić M, Schneider K, Hornfeck R (2016) A case study on the capability of rapid tooling thermoplastic laminating moulds for manufacturing of CFRP components in autoclaves. Procedia CIRP 50:390–395. https://doi.org/10.1016/j.procir.2016.04.151

42. Rodríguez-Parada L, Mayuet PF, Gámez AJ (2019) Industrial product design: study of FDM technology for the manufacture of thermoformed prototypes. Proc Manuf 41:587–593. https://doi.org/10.1016/j.promfg.2019.09.046

43. Bere P, Neamtu C, Udroiu R (2020) Novel method for the manufacture of complex cfrp parts using fdm-based molds. Polymers 12(10):1–20. https://doi.org/10.3390/polym12102220

44. Murdy P, Dolson J, Miller D et al (2021) Leveraging the advantages of additive manufacturing to produce advanced hybrid composite structures for marine energy systems. Appl Sci (Switzerland) 11(3):1–15. https://doi.org/10.3390/app11031336

45. Hassen AA, Lindahl J, Chen X, et al (2016) Additive manufacturing of composite tooling using high temperature thermoplastic materials. In: SAMPE conference proceedings, Long Beach, CA, https://www.researchgate.net/publication/324442073

46. Kunc V, Lindahl J, Dinwiddie R, et al (2016) Investigation of in-autoclave additive manufacturing composite tooling. In: CAMX conference proceedings, Anaheim, CA, http://energy.gov/downloads/doe-public-access-plan

47. Grassi M, Smith F (2019) Aerospace composite technology roadmapping. In: Composites Leadership Forum

48. Zheng X, Lee H, Weisgraber TH et al (2014) Ultralight, ultrastiff mechanical metamaterials. Science 344(6190):1373–1377. https://doi.org/10.1126/science.1252291

49. Schaedler TA, Jacobsen AJ, Torrents A et al (2011) Ultralight metallic microlattices. Science 334(6058):962–965. https://doi.org/10.1126/science.1211649

50. Lu TJ, Stone HA, Ashby MF (1998) Heat transfer in open-cell metal foams. Acta Materialia 46(10):3619–3635. https://doi.org/10.1016/S1359-6454(98)00031-7

51. Catchpole-Smith S, Sélo RR, Davis AW, et al (2019) Thermal conductivity of TPMS lattice structures manufactured via laser powder bed fusion. Additive Manufacturing 30(August):100,846. https://doi.org/10.1016/j.addma.2019.100846

52. Goransson P (2006) Acoustic and vibrational damping in porous solids. Philosophical Transactions of the Royal Society A: Mathematical, Physical and Engineering Sciences 364(1838):89–108. https://doi.org/10.1098/RSTA.2005.1688

53. Brown JA, Bishop JE, Brennan-Craddock J, et al (2012) The design of impact absorbing structures for additive manufacture. Journal of Physics: Conference Series 382(012042). https://doi.org/10.1088/1742-6596/382/1/012042

54. McConaha M, Anand S (2020) Design of stochastic lattice structures for additive manufacturing. International Manufacturing Science and Engineering Conference 1:1–11. https://doi.org/10.1115/MSEC2020-8439

55. Groth JH, Anderson C, Magnini M et al (2022) Five simple tools for stochastic lattice creation. Additive Manufacturing 49(102):488. https://doi.org/10.1016/J.ADDMA.2021.102488

56. Maliaris G, Sarafis E (2016) Mechanical behavior of 3D printed stochastic lattice structures. Solid State Phenomena 258:225–228. https://doi.org/10.4028/www.scientific.net/SSP.258.225

57. Ashby MF, Evans AG, Fleck NA, et al (2000) Metal foams: a design guide. Butterworth-Heinemann, Woburn, http://www.bh.com

58. Martínez J, Song H, Dumas J, et al (2017) Orthotropic k-nearest foams for additive manufacturing. ACM Trans Graph 36(4). https://doi.org/10.1145/3072959.3073638ï, https://hal.archives-ouvertes.fr/hal-01577859

59. Goguelin S (2022) 3D printing in orthopedics: better knee, hip & spine implants. https://all3dp.com/1/3d-printing-orthopedics-knee-hip-spine-implants/

60. Kondjoyan A, Péneau F, Boisson HC (2002) Effect of high free stream turbulence on heat transfer between plates and air flows: a review of existing experimental results. Int J Ther Sci 41(1):1–16. https://doi.org/10.1016/S1290-0729(01)01299-6. www.sciencedirect.com/science/article/pii/S1290072901012996

61. Choy SY, Sun CN, Leong KF et al (2017) Compressive properties of functionally graded lattice structures manufactured by selective laser melting. Mater Des 131:112–120. https://doi.org/10.1016/J.MATDES.2017.06.006

62. Mukhopadhyay T, Adhikari S (2017) Effective in-plane elastic moduli of quasi-random spatially irregular hexagonal lattices. Int J Eng Sci 119:142–179. https://doi.org/10.1016/J.IJENGSCI.2017.06.004

63. Yin H, Huang X, Scarpa F et al (2018) In-plane crashworthiness of bio-inspired hierarchical honeycombs. Composite Structures 192:516–527. https://doi.org/10.1016/J.COMPSTRUCT.2018.03.050

64. Gen3D (2021) Sulis V1.9.10

65. Develop3D (2022) Gen3D rolls out Sulis V1.10. https://develop3d.com/cad/gen3d-rolls-out-sulis-v1-10/

66. Mathworks Inc. (2020) MATLAB 2020b

67. Synopsys (2021) Simpleware ScanIP v2021

68. Dassault-Systems (2020) ABAQUS v2020

69. Jahns K, Bappert R, Böhlke P et al (2020) Additive manufacturing of CuCr1Zr by development of a gas atomization and laser powder bed fusion routine. Int J Adv Manuf Technol 107(5–6):2151–2161. https://doi.org/10.1007/s00170-020-04941-7

70. Du Y, Mukherjee T, Finch N et al (2022) High-throughput screening of surface roughness during additive manufacturing. J Manuf Process 81(June):65–77. https://doi.org/10.1016/j.jmapro.2022.06.049